Nocturnal Low-Level Jet Characteristics observed during CASES-99

R.M. Banta[1], R.K.Newsom[2], J.K. Lundquist[3], Y.L. Pichugina[2], R.L. Coulter[4] and L.D. Mahrt[5]

[1]Environmental Technology Laboratory/NOAA, Boulder, Colorado, USA
[2]Cooperative Institute for Research in the Atmosphere, Ft. Collins, Colorado, USA
[3]Program in Atmospheric and Oceanic Sciences, University of Colorado, Boulder, USA
[4]Argonne National Laboratory, IL
[5]College of Oceanic and Atmospheric Sciences, Oregon State University, Corvallis, USA

Abstract

A combination of high-resolution Doppler lidar (HRDL), a 60-m instrumented tower, and a triangle of three Doppler-mini-sodar/profiler combinations was used to study the low-level jet (LLJ) over south-central Kansas during the CASES-99 field campaign. Using this collection of instrumentation we have determined the speed U_X, height Z_X, and direction D_X of the LLJ. We investigate here the frequency of occurrence, the spatial distribution, and the evolution through the night, of these LLJ characteristics. The jet of interest in this study was that which affects the shear and turbulence below the jet and near the surface, and thus was the lowest wind maximum. We found that this wind maximum, which was most often between 7 and 10 m s^{-1}, was generally at or below 100 m AGL as measured by HRDL at the CASES central site; this height is below the minimum range of current-generation profilers. Over the 60km array, the topography varied by ~100 m. The wind speed and direction were relatively constant over this distance (with some tendency for stronger winds at the highest sight) but Z_X was more variable. Although Z_X was occasionally about equal at all 3 sites, indicating that the jet was following the terrain, more often it was not. The LLJ often seemed to be relatively level, i.e., at the about same height MSL, although the vertical resolution of the profiler was too coarse to determine this definitely. In the behavior of the LLJ with time through the night, Z_X was again more variable than U_X, and on some nights U_X was remarkably steady. Lidar scan data available at fine time resolution (~30 s) showed episodes of short-period (several minutes) fluctuations of both U_X and Z_X. Two nights with strong turbulence below jet level were further investigated using the 60-m tower at the main CASES-99 site. Evidence of TKE increasing with height and downward turbulent transport of TKE indicates turbulence being primarily generated aloft and mixing downward, supporting the upside-down boundary layer notion in the SBL.

1. Introduction

One of the most important processes in the evening boundary-layer transition over relatively flat terrain is the action of cooling at the ground in decoupling the flow just above the surface from surface friction. This decoupling disrupts the daytime balance of forces in the horizontal and produces acceleration of the flow above the atmospheric surface layer in a manner well described by Blackadar (1957). The acceleration produces a layer–extensive in the horizontal but shallow in the vertical–of high-momentum air, which exhibits a maximum or nose in the vertical profile of the horizontal wind. This maximum has been called a low-level jet (LLJ).

The term LLJ has been used to refer to any low-level speed maximum in the vertical profile of the wind, and LLJ's can be produced by a number of mechanisms, which has led to ambiguity in the usage of this term in the literature. For example, density currents (including synoptic cold fronts, thunderstorm gust fronts, drainage-flow fronts, sea-breeze fronts, etc.) have an LLJ profile in the cold-air layer behind the front (Bowen 1996), and Whiteman et al. (1997) found in their LLJ climatology that most wind maxima that fit their criteria for an LLJ and had a northerly component were post-cold-frontal jets (and therefore large-scale density currents). LLJ climatologies show a percentage of LLJ's occurring during daylight hours, and these would not be due to Blackadar's mechanism. Even nocturnal LLJ's can have different causes and scales of geostrophic pressure gradients. For example, in the nocturnal LLJ of the Great Plains of the United States, which has been extensively studied because of its impact on severe weather, the relevant pressure gradient has been ascribed either to baroclinity due to the sloping terrain or to the synoptic gradient associated with the Bermuda high-pressure system, both of which produce a geostrophic wind from a southerly direction.

In the present study we are concerned with the nocturnal LLJ that has a role in generating shear and turbulence between the level of maximum wind speed Z_X and the earth's surface, and thus influences, and sometimes probably controls, surface-atmosphere exchange at night. Hence, we are interested in the lowest LLJ maximum that forms due to Blackadar's mechanism. The CASES-99 dataset that we are using for this study typically showed a single-level jet maximum, but many instances of multiple LLJ maxima also occurred (Fig. 1). Even more significantly, Z_X for this central Kansas site was frequently at or below 100 m above ground level (AGL). The importance of this finding is that this level is below the minimum range of current-generation radar wind profilers, including the 915 MHz boundary-layer systems, and thus these jets are undetectable by those instruments. Instrument capability is an important aspect of the nocturnal LLJ problem, and we address this issue later in this study.

The instrumentation used in this study includes 915-MHz profilers, mini sodars, a 60-m meteorological tower, and the High-Resolution Doppler Lidar (HRDL) developed and deployed by the Environmental Technology Laboratory (ETL) of the National Oceanic and Atmospheric Administration (NOAA). Previous studies of nocturnal LLJ's have been handicapped by coarse sampling in space and time, as pointed out by Whiteman et al. (1997), Lundquist (2000), and others. Profiles taken by HRDL were available at time intervals of $\lesssim 1$ min with vertical resolutions of $\lesssim 10$ m for much of entire nights, allowing the evolution of the nocturnal LLJ to be described in unprecedented detail. Grund et al (2001) had previously shown that HRDL is ideally suited to studying the LLJ (see their Fig. 9). The purpose of the present study is to

describe the characteristics, including speed, height, and direction, of LLJ's observed during CASES-99. We use the datasets to determine the distributions of the frequency of occurrence of these characteristics, their spatial variability, and their behavior as a function of time through the night. We show examples of the relationship between LLJ evolution and near-surface turbulence generation and mixing, which have been shown to be important consequences of LLJ formation (Smedman 1988, Mahrt 1999). More detailed case studies are in progress.

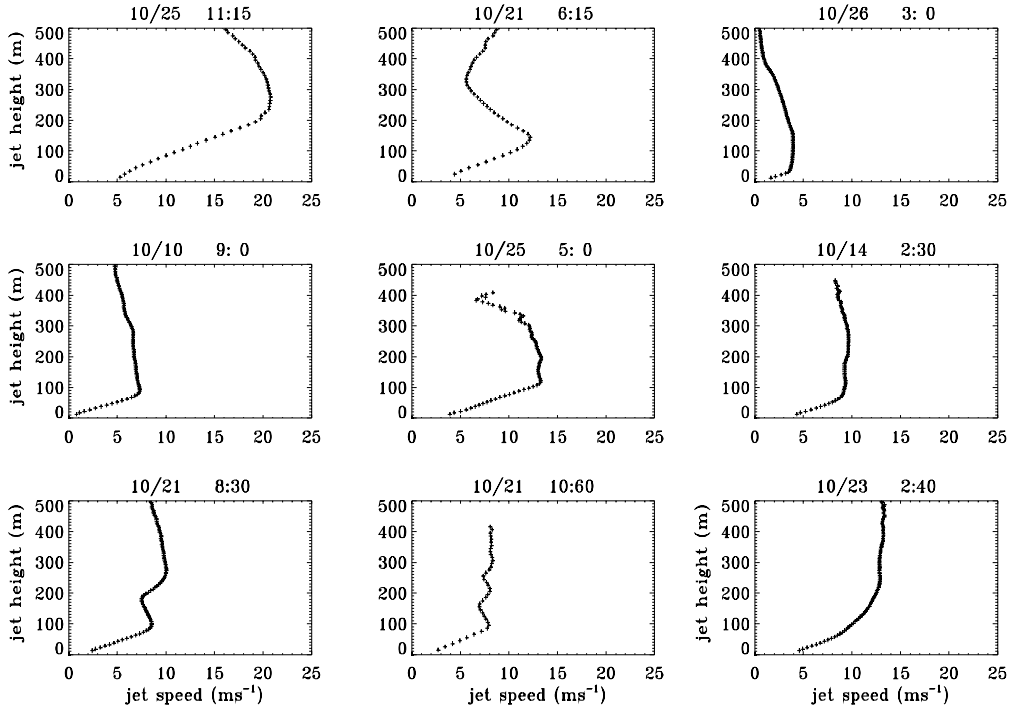

Figure 1: Sample LLJ profiles either from HRDL vertical-slice scans or from VAD scans. The lowest wind-speed maximum in each case except the last one was classified as a LLJ in this study. The last profile was not classified as a LLJ.

2. Instrumentation and analysis procedures

The Cooperative Surface-Atmosphere Exchange Study field campaign of October 1999 (CASES-99) was an intensive study of the nocturnal stable boundary layer (SBL). Poulos et al. (2001) describe the objectives, instrumentation, and venue in detail. CASES itself is a long-term, interdisciplinary study of meteorological and hydrological processes in the Walnut River watershed in southeast Kansas just east of Wichita. The backbone of CASES is a long-term deployment by Argonne National Laboratory (ANL) of 915 MHz radar wind profilers with minisodars, and other instrumentation including surface mesonet stations, called the Atmospheric Boundary Layer Experiments (ABLE) array (LeMone et al. 2000). ABLE includes a triangle of sodar/profiler sites surrounding the CASES-99 main site near the town of Leon, where HRDL

was located at an elevation of 434 m (scanner height). These sodar/profilers were at the following locations as shown in Fig. 2. Beaumont (BEA), in the northeast corner of the watershed, is the highest station at an elevation of 460 m MSL. The eastern site, Whitewater (WHI), has an elevation of 420 m. The southern Oxford (OXF) site is the lowest of the three at an elevation of 360 m MSL.

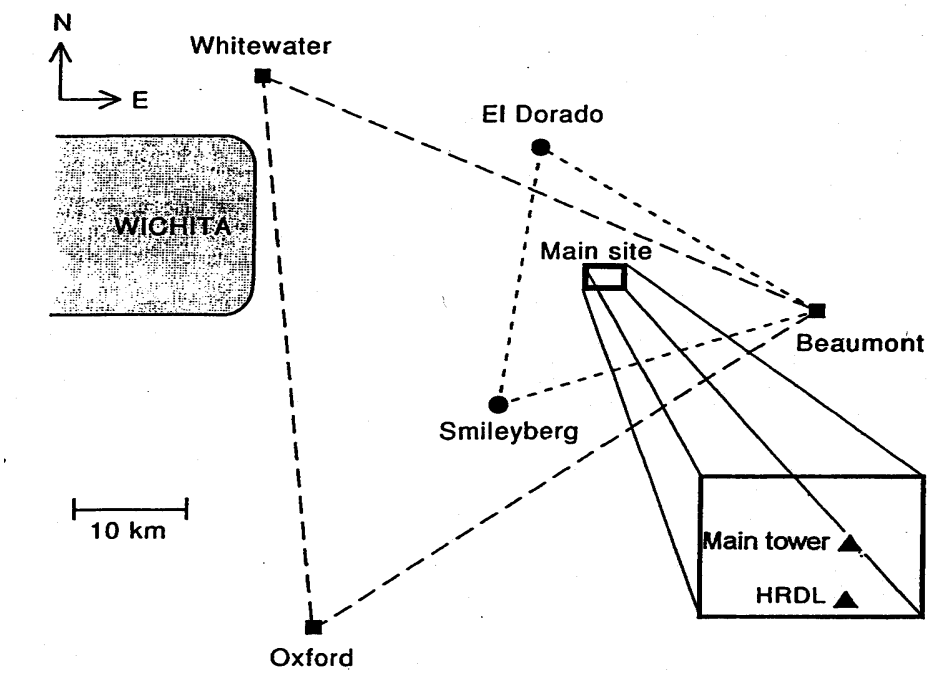

Figure 2. Map of the study area showing the CASES-99 main site (black dot) near Leon KS, and the locations of the three sodar/profiler sites (+).

During each night of CASES-99, at least four and sometimes more than 20 rawinsondes were launched from various sites within the CASES-99 instrument array. These rawinsondes rely on a connection with Global Positioning System (GPS) satellites for position-finding and wind-finding. Of the 238 nocturnal (0000-1400 UTC) soundings taken during CASES-99, 165 lost their connection with the satellites upon launch, and thus were unable to provide winds in the lowest 100 m at least (Lundquist et al. 2000) before reaquiring connection. These data outages prevent any systematic study of the nocturnal low-level jet as revealed by the GLASS soundings. Whiteman et al. (1997) also evaluated the first-reported wind measurement above the surface for the special rawinsonde ascents for 2 years at the CART site in north-central Oklahoma, where the sondes were tracked by LORAN. They found that the first wind was below 100 m 83% of the time, with the majority at 50-70 m. Because at least a couple of points below Z_X are needed to define an LLJ, it is likely that many jets important to our study would be missed even by these carefully controlled rawinsonde data. Thus, for applications such as ours, where LLJ maxima below 100 m AGL are of interest, one must use caution in interpreting LLJ climatologies based

on profiler or rawinsonde datasets.

2.1 LLJ CRITERIA

Vertical profiles of the horizontal wind speed were determined using procedures described in the following subsections. Examples of some types of profile we found are shown in Fig. 1. We identified LLJ's both by visual inspection of each profile, and, to remove subjectivity, also using an objective, automated technique. The objective criteria we chose to define a LLJ were based on those of Andreas et al. (2000), which called for choosing those low-level wind-speed maxima that exhibited a decrease of at least 2 m s^{-1} at vertical levels both above and below the level of the peak value Z_X. Criteria used by Bonner (1968) and Whiteman (1997) led to excluding many jets that we felt obviously belonged in our sample, given the objectives of the study; for example, profiles resembling Figs. 1c-h were rejected by these criteria, but are of interest for this study. Even using the Andreas criteria, we found as a result of the visual-inspection process that we were excluding an unacceptably large number of LLJ's. Given the precision of HRDL and the fine vertical resolution in the calculated mean profiles, we felt justified in using smaller vertical threshold criteria of 1.5, 1.0, and 0.5 m s^{-1}, and we found that 0.5 m s^{-1} gave the best agreement with visual determinations. However, because we also used sodar/profiler results, where we were not confident in using a difference of 1.0 m s^{-1} or lower, we used a threshold of 1.5 m s^{-1} for the sodar/profiler datasets.

2.2 HIGH-RESOLUTION DOPPLER LIDAR

HRDL is a scanning Doppler lidar system capable of mapping out the Doppler velocity field in the boundary layer with a range resolution of 30 m and a velocity precision of $\lesssim$10 cm s^{-1}. Operating characteristics of HRDL are shown in Table 1.

Table 1. Performance characteristics for HRDL.

Wavelength	2.02μm
Range Resolution	30m
Pulse Repetition Frequency	200Hz
Beam Rate	≤8Hz
Minimum Range	250m
Maximum Range	2-6km
Velocity Accuracy	10cm s^{-1}
Maximum scan rate	60 ^{o} s^{-1}

More details can be found in Grund et al. (2001) and Wulfmeyer et al. (2000), and its role in CASES-99, in Blumen et al. (2001), Newsom and Banta (2001), and Poulos et al. (2001). In this study we use both azimuth and elevation scanning capability of HRDL.

To reduce the effects of poor signal quality and hard-target returns on profiles derived from the Doppler velocities, the data were quality controlled. While scanning at low elevation angles, the lidar beam occasionally intersects hard targets such as trees, towers, power lines, terrain, etc. This results in large return signals that must be filtered out before processing the data. In addition to the large return, such hard target returns are also identified by Doppler velocities which are close to zero. In the weak signal regime Doppler frequency estimates become uniformly distributed throughout the pass band. These estimates are easily identified by small return signals, and we have filtered them out by thresholding based on the return signal level.

2.2.1 *Modified Velocity-Azimuth Display*

During periods of operation HRDL performed a variety of different scans as opposed to a routine schedule of scans. As a result, the dataset consists of various scan types with various durations. To retrieve a regular sampling of vertical wind profiles from the lidar dataset, we developed an algorithm very similar to the conventional velocity-azimuth display (VAD) technique (Browning and Wexler 1968). Unlike the conventional VAD method, which uses only full 360^o azimuth scans, the modified VAD approach makes use of data from a variety of scan types. This new algorithm involves only a slight modification to the conventional VAD processing technique.

In this new method Doppler radial velocity u_r data acquired during a given time period are divided into 10 m vertical bins. A given bin may contain u_r measurements scattered over a distribution of azimuth and elevation angles, depending on the scans performed during that period. It is assumed that within a vertical bin the mean wind is uniform and horizontal. The components of the mean wind, U and V within a vertical bin are obtained by minimizing the total squared deviation between the radial component of the mean velocity and the u_r measured by the lidar. This processing technique was applied to the entire HRDL CASES-99 data set using a 30-min averaging period oversampled at 15-min intervals.

The linear system that results from least squares minimization has no solution if, during the averaging period, all of the azimuth angles are the same. Furthermore, the system will be ill-conditioned if the difference between the minimum and maximum azimuth is small. Mean-wind estimates derived from ill-conditioned linear systems as well as very noisy data are excluded based on quality parameters, which are proportional to the computed error in the retrieved mean velocity components. The quality parameters provide an objective method of rejecting bad estimates.

We found the height of the maximum wind speed for each averaging period and noted the time, and the speed U_X, the direction D_X, and the height Z_X of the jet maximum.

2.2.2 *Vertical cross sections*

Sector scans in elevation produced vertical slices or cross sections of u_r. These scans often took 20-35 s to complete and were often performed repeatedly for animation during the analysis.

It was thus typical to have 50-100 such scans per hour, interspersed with VAD-type scans.

Vertical-slice scans were often performed looking approximately into or along the mean wind vector. As result, in situations where directional shear was not significant, profiles of the mean velocity component derived from vertical-slice scan data differs little from the mean wind profile obtained from the modified VAD algorithm described in the previous section. Profiles of the mean velocity component *U(z)* parallel to the scan plane and its variance $\overline{u'^2(z)}$ were computed from vertical slice scans as follows.

The horizontal component (parallel to the scan plane) was estimated from u_r measurements by dividing by the cosine of the elevation angle. This provides a good approximation to the horizontal component if the vertical velocity component is much less than the horizontal component and if the scan elevation is small. Horizontal velocity profiles derived from individual vertical-slice scans were obtained by sorting the data into 10-m vertical bins. Within each bin, estimates of the mean and variance were obtained by averaging horizontally. Variance estimates are much more sensitive to measurement error than are the means. Distributions are significantly broadened by measurement error which increases with range from the lidar due to weakening return signals.

Each vertical-slice scan thus provides a vertical profile of *U(z)* and $\overline{u'^2(z)}$. At this point we could plot each profile on a time-height cross section of mean wind and wind-speed variance. This was done for each of the 12 nights when HRDL had good data. An example is given in Fig. 3. Similar to the VAD procedure, we found the level of the jet maximum, then noted the time, the height Z_X, and the speed U_X for each vertical-slice scan (direction was not available from these scans). These data too were further averaged over 15-min intervals.

2.3 PROFILER/MINI-SODAR COMBINATION

Boundary-layer radar-wind profilers (Eklund et al., 1988) provide wind profiles by transmitting a radar signal at 915 MHz and measuring the Doppler-shifted frequency of the backscatter from one vertical beam and two or four offset beams. Six min are required for one scan sequence; multiple scans are averaged together to create hourly averages of winds. These hourly averages are considered reliable to within ±1 m s^{-1}. The lowest level for which winds are available is typically ~150 m, and range gates are 60 m deep.

In the CASES-99 field program, three boundary-layer wind profilers were operated by the Argonne Boundary Layer Facility (Coulter et al. 1999b). These profilers were co-located with sodars. Additionally, two boundary-layer profilers were operated by the National Center for Atmospheric Research, but these sites collected no wind data below the lowest profiler range gate, so they are not included in this study.

The wind profiler data provided by Argonne National Laboratory (ANL) have undergone quality control by that laboratory. Prior to any analysis, remaining outliers among the boundary-layer wind profiler data (caused by "ringing" or instrument noise in the profiler) were removed, and the approximately hourly (and sometimes half-hourly) data have been interpolated onto a regular hourly grid.

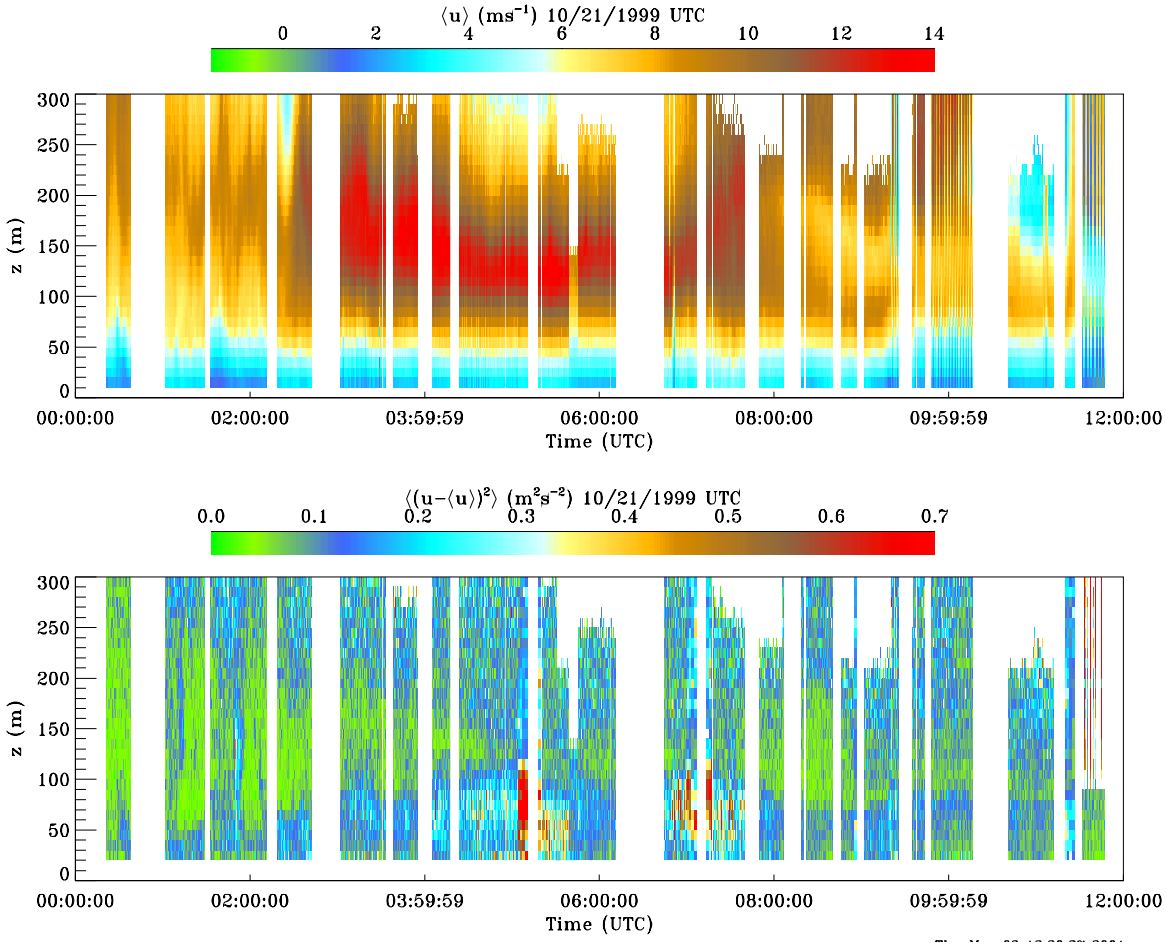

Figure 3: Sample time-height cross sections of mean wind speed (top panel) and variance of the radial wind component (bottom panel) calculated from HRDL vertical-slice scans. Each vertical line represents a vertical profile of the horizontally averaged wind speed or variance from the vertical cross sections, as described in the text.

Three Doppler minisodars, co-located with the ANL boundary-layer profilers, were deployed both to provide a high-resolution wind profile between the surface and the lowest level of the boundary-layer profilers and to verify the lowest levels of the profilers (Coulter et al., 1999b). Sodars rely on the transmission of sound, and thus the sodar signal is directly dependent on the temperature and wind structure of the atmosphere. The sodars have a 5-m range gate and are designed to collect data between 10 and 200 m; 15-minute averages of these data are provided by ANL. For this study, these 15-minute averages were further averaged into hourly profiles for better compatibility with the profiler data.

3. LLJ Frequency Distributions: Speed, Height, Direction

For many applications, and for assessing the representativeness of the CASES-99 dataset, the frequency of occurrence of speed U_X, height Z_X, and of the direction of the LLJ (D_X), are important. We used the 15-min HRDL data and 1-h sodar/profiler data to generate histograms of these quantities. The two datasets are described separately to assess the similarities and differences due to the different instrumentation.

Histograms based on HRDL 15-min means of U_X, Z_X, and D_X are shown in Fig. 4.

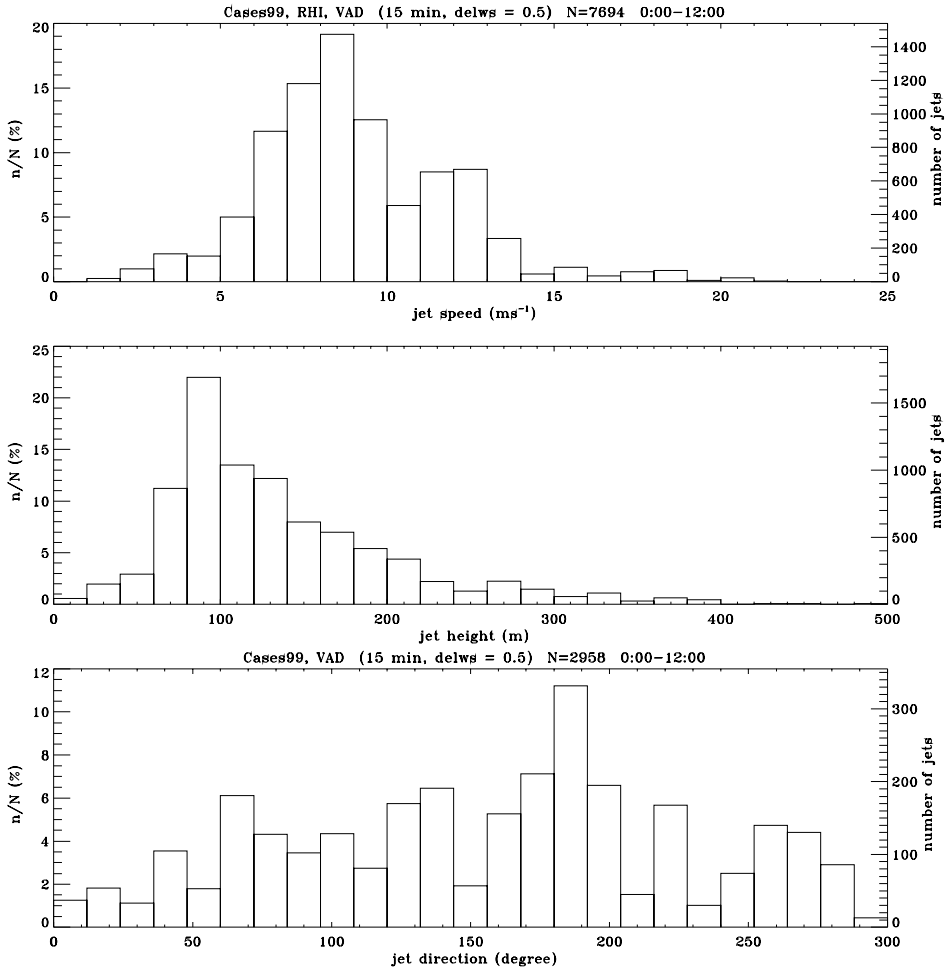

Figure 4: Histograms of jet speed U_X (top panel), height Z_X of maximum speed (middle panel), and direction of jet maximum D_X (bottom). Data were compiled from 15-min meansof each quantity determined from HRDL vertical-slice and VAD-type scans. Percentages of occurrences in each bin are shown along left vertical axis, and total number of occurrences in each bin is indicated along the right vertical axis.

Most of the speeds of the jet maxima fell between 7 and 10 m s^{-1}, with a mode of nearly 19% of the occurrences at 8-9 m s^{-1}. The fact that the height of the LLJ's fell mostly around 100 m means that our Z_X's are lower than in most other studies in the U.S. Great Plains. In the most recent study, for example, Whiteman (1997) found peaks in occurrence during both warm and cold seasons at 300-400 m AGL. To a large degree these differences reflect differences in study objectives and therefore in the definition of LLJ, but some of the differences are also instrumental: HRDL is ideally suited to detect Z_X in the 50-150-m range, whereas profiler data are unavailable or unreliable at these altitudes, and rawinsonde data using LORAN or GPS often have problems aquiring signal until the sonde is well into or through this layer, as described in the previous section. D_X was distributed over all quadrants, but showed a strong peak for southerly jets.

As an extension of the histogram analysis, we also plotted cumulative frequency distributions (Fig. 5) and a plot of Z_X vs. U_X (Fig. 6). The cumulative distributions show, e.g., that 40% of the jet maxima occurred below 100 m and 67%, below 140 m. The Z_X vs. U_X plots show a modest tendency for the stronger LLJ's to occur at higher levels than the weaker ones, for this dataset.

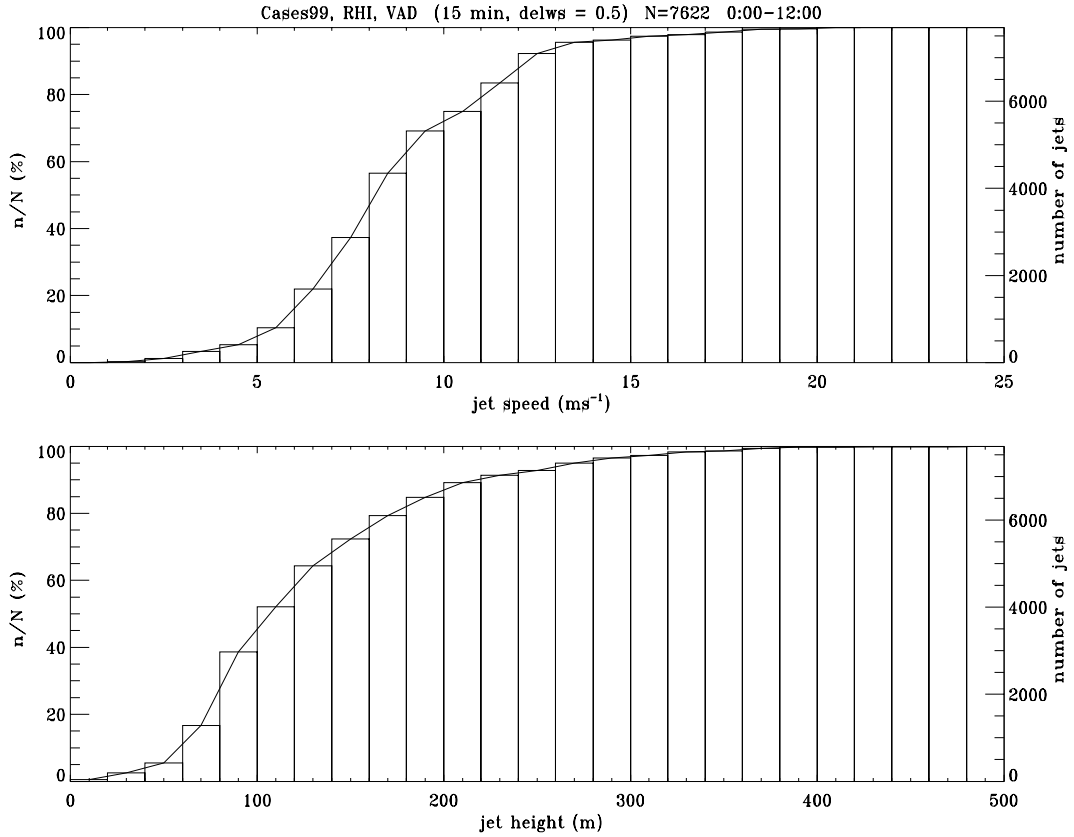

Figure 5: Cumulative distributions of U_X (top panel) and Z_X (bottom panel) based on data from Fig. 4. Vertical axes are as in Fig. 4, except for cumulative-distribution statistic.

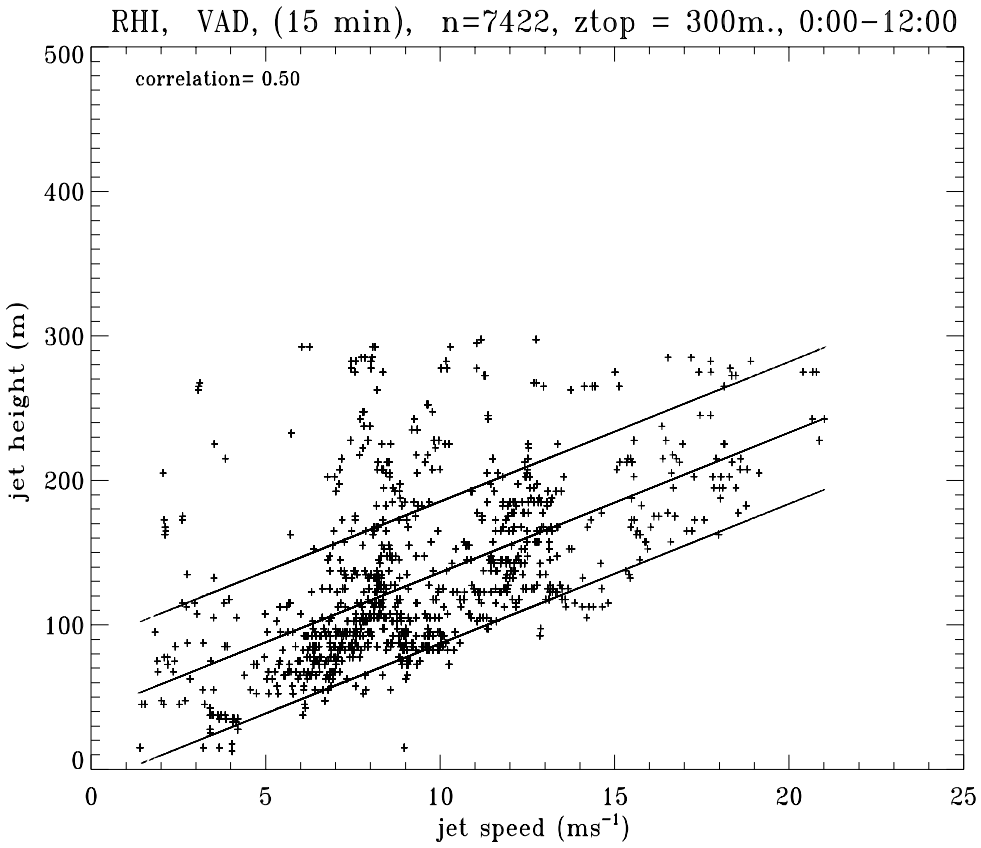

Figure 6: Scatter diagrams of Z_X vs. U_X from the same data as in Fig. 4, taking only those values where Z_X < 300 m. Middle line represents best-fit linear regression (R=0.50) and upper and lower lines are for ±1 standard deviation.

Histograms from the sodar/profiler data (Fig. 7-9) are given for each of the 3 sites. Jet speeds were broadly consistent with the 7-10 m s^{-1} concentration in the HRDL data, but WHI showed a peak at lower wind speeds (4-6 m s^{-1}), and BEA showed significant occurrences of stronger U_X of 14-20 m s^{-1}. Z_X at BEA was similar to the HRDL data near Leon, with a peak at ~80-100 m AGL. Both WHI and OXF had peak occurrences somewhat higher at 120-140 m AGL. A major difference in the sodar/profiler Z_X data is the indication of more occurrences of maxima above 200 m, which would have been measured by the profiler. Profiler data, indicated by shading in the three figures, appear quantized in the histograms, because of the 60-m range-gate spacing. The peak in LLJ direction at all 3 profiler sites was southerly, in agreement with the HRDL data.

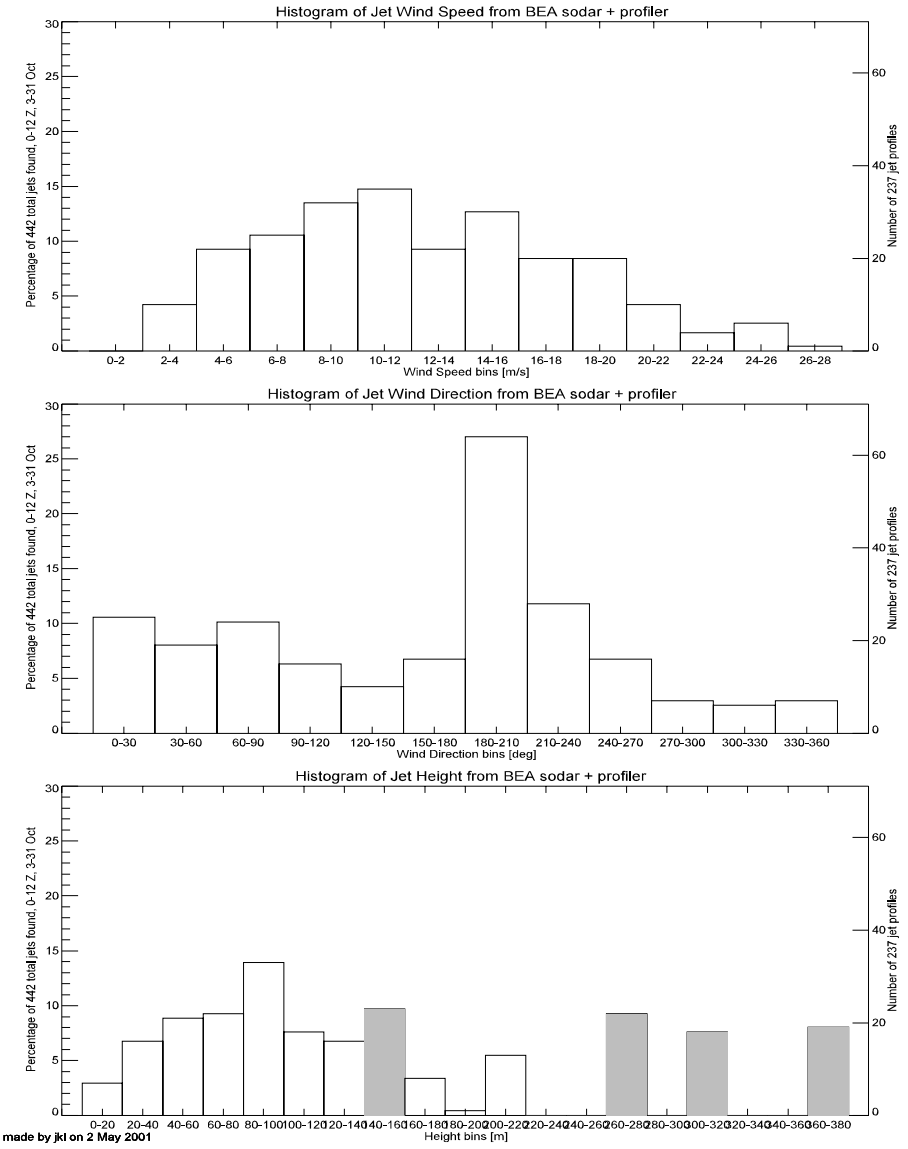

Figure 7: Distributions of the characteristics of LJs identified in data from the Beaumont (BEA) sodar/profiler from 0000 - 1200 UTC, 3-31 October. Top panel depicts the distribution of wind speeds U_X at jet maximum. The middle panel shows the distribution of wind directions D_X at jet maximum (0 degrees is from the north). The bottom panel illustrates the distribution of the height levels at which the jet was observed Z_X. Shaded bars indicate the levels of the profiler range gates, which are 60 m deep and lead to some quantization of jet heights. For example, the bar at 240-260 m is based on the profiler range gate at 260 m and thus represents heights from 230-290 m. The bar at 140-160 m includes both the lowest profiler range gate at 145 m and sodar data.

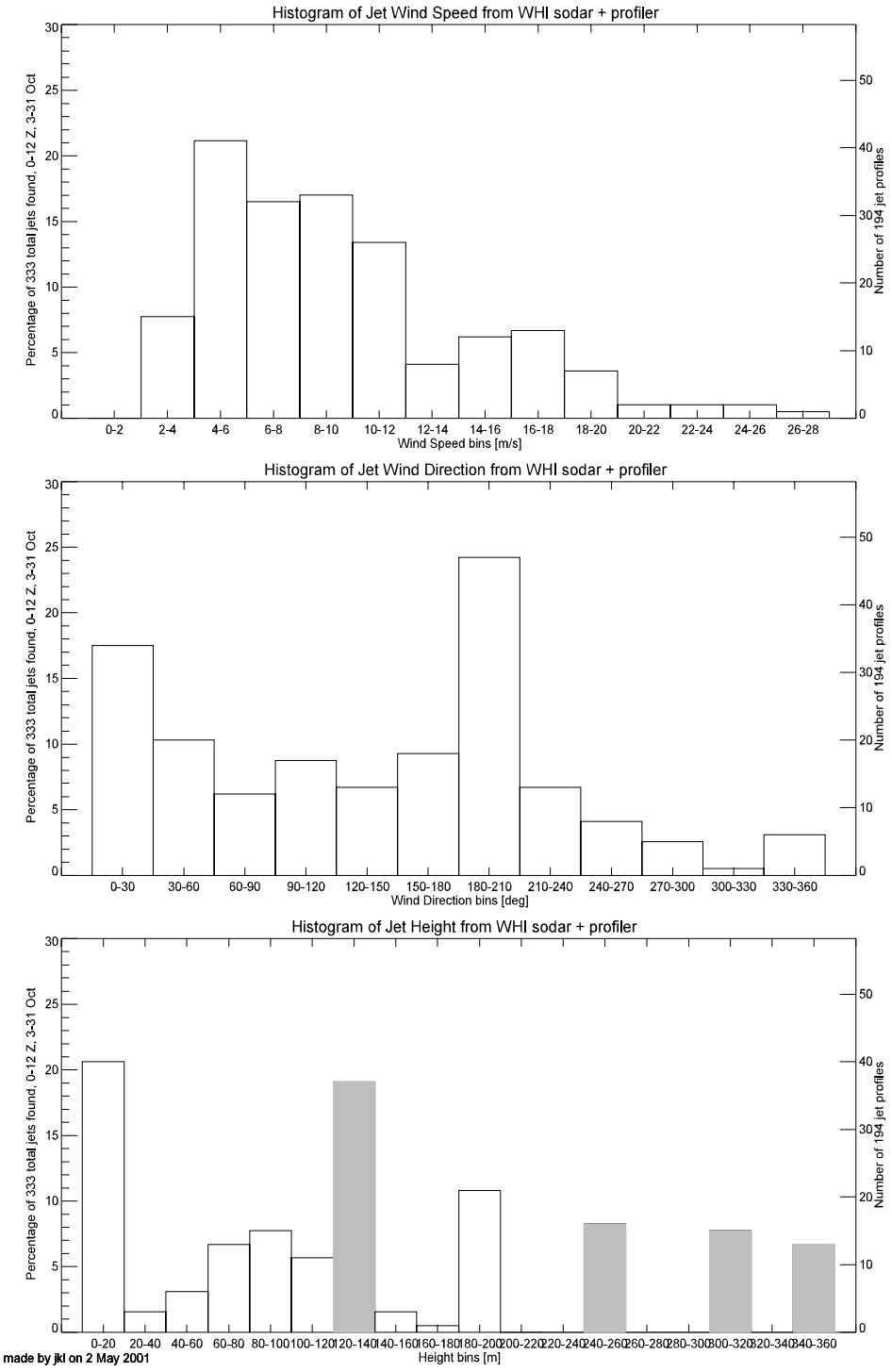

Figure 8: As in Figure 7, but of data from the Whitewater (WHI) site. The lowest profiler range gate at Whitewater was at 137 m AGL.

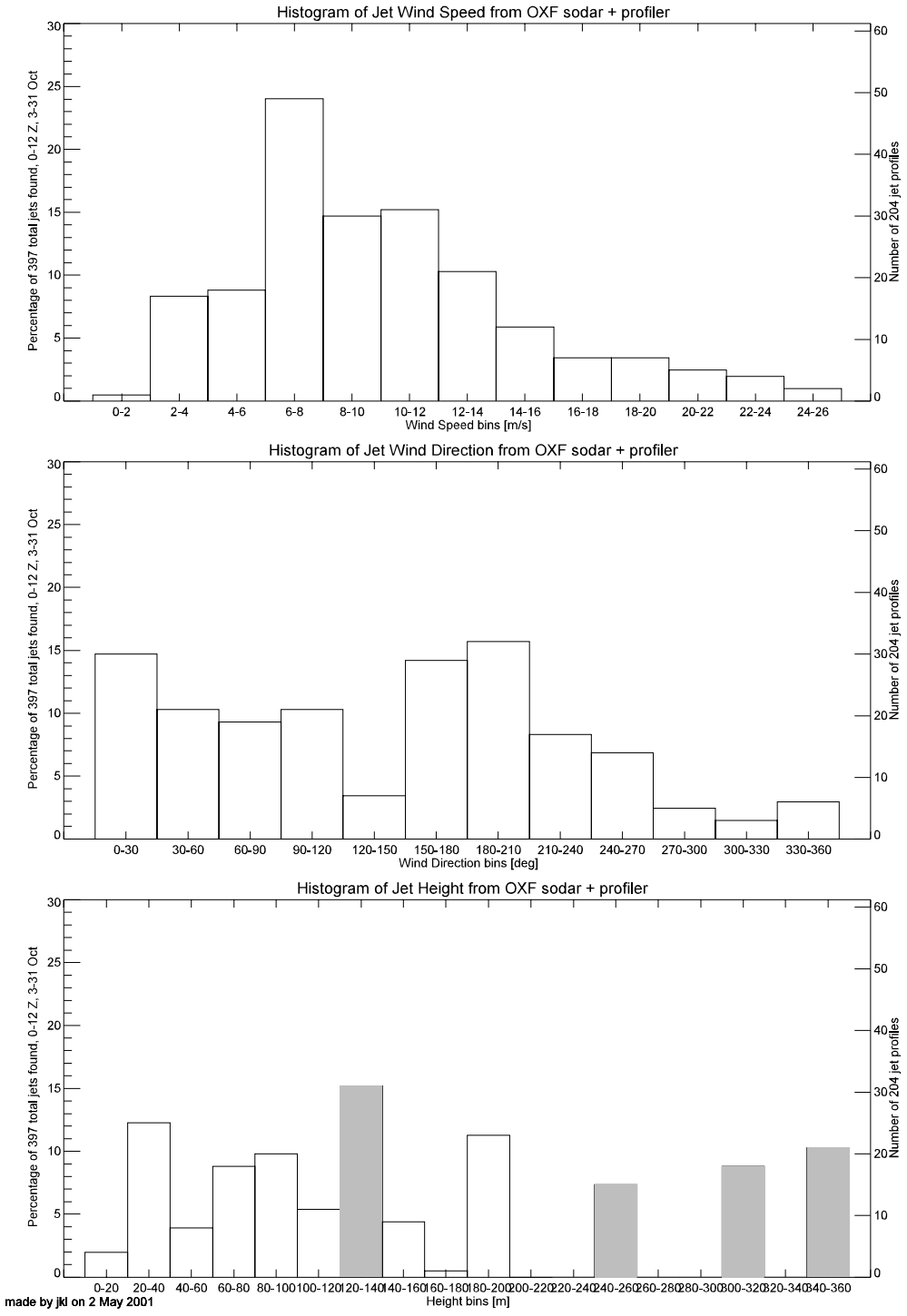

Figure 9: As in Figure 8, but of data from the Oxford (OXF) site. The lowest profiler range gate at Oxford was at 137 m AGL.

The histograms in Figs. 7-9 indicate variations in U_X, D_X, and Z_X between the three sites. To determine if these variations are due to unequal sampling between the profilers or due to a physical phenomenon (such as the jet remaining at a constant height above sea level rather than above the local topography), we examine a set of 102 hourly nocturnal profiles where all three sites showed a jet profile using the Andreas 1.5 m s^{-1} criterion. The variations between the sites were calculated as an hourly spread: for each of the 102 hourly profiles, the spread is calculated as the difference between the maximum and minimum of the 3 values. We also examined a subset of 5 nights with the best percentage of data returned (9, 11, 14, 21 and 24 October).

We find little variation in U_X and D_X across the watershed. For the large set, the average spread in the wind speed was 2.9 m s^{-1}, with a standard deviation of 2.5 m s^{-1}. As the profiler accuracy is on the order of 1 m s^{-1}, we find this to be good agreement. The subset of 5 nights shows similar agreement, with a mean spread of 2.9 m s^{-1} and a standard deviation of 1.9 m s^{-1}. The Beaumont site (BEA) had a slight preference for stronger jets: 40.2 % of the profiles showed the strongest jet at BEA, whereas WHI showed the strongest jet in 30.4 % of the 102 profiles, and OXF showed the maximum jet U_X 29.4 % of the time. The preference for strong jets at BEA is enhanced in the 5-night subset: the strongest jets are at BEA in 53%, WHI in 21 %, and OXF in 26% of the profiles.

The variability in jet wind direction across the watershed was similarly small. For the entire nocturnal CASES-99 dataset, the average spread in D_X was 6.5 degrees; for the subset of 5 nights, the average spread in wind direction was 7.2 degrees. Because a typical wind profile shows much larger variations in wind direction over the lowest 200 m, we find this agreement between stations to be excellent.

A discussion of the variation in jet height over the watershed is more problematic due to the nature of sodar and profiler data. If a jet were located above the top of the sodar data (200 m at best sodar performance but more often near 100 or 120 m), the Z_X would be measured by the profilers, and the difference between the station elevations is on the order of the range gates of the profilers (60 m). Additionally, errors in estimating the jet height may be introduced when the jet maximum falls in a data-sparse region of the profile, where vertical resolution is coarse. Given these caveats, the data indicate that the LLJ height did not in general follow the local terrain slope, because the measured differences between Z_X on individual nights was usually significant. The station with the highest elevation, BEA, tended to have the lowest Z_X--on 62% of the time on all nights, and 65% of the time on the five selected nights. The lowest site at OXF, exhibited the highest Z_X on 43.1% of the hourly intercomparisons for all nights and 39.5% of the profiles on the selected nights. This suggests that the height of the LLJ could be level (i.e., at a constant height MSL), but the coarse vertical resolution of the measurements and the smallness of the sample size prevent confirming this. Two specific examples where the jet was well defined at all 3 sites are shown in Fig. 10. In the first case (14 Oct 0400 UTC) the jet was level, and in the second (11 Oct 0700 UTC) it followed the topography. 14 Oct, the night of hte first example, was interesting, because Z_X at all 3 sites started out at the same height AGL (i.e., terrain following) for several hours after sunset, and then became level (at same height MSL) later in the night. The sodar/profiler data for all nights are being studied in greater detail for these effects. Further information on the relative Z_X's at each of the sites is given in the time series plots in the next section.

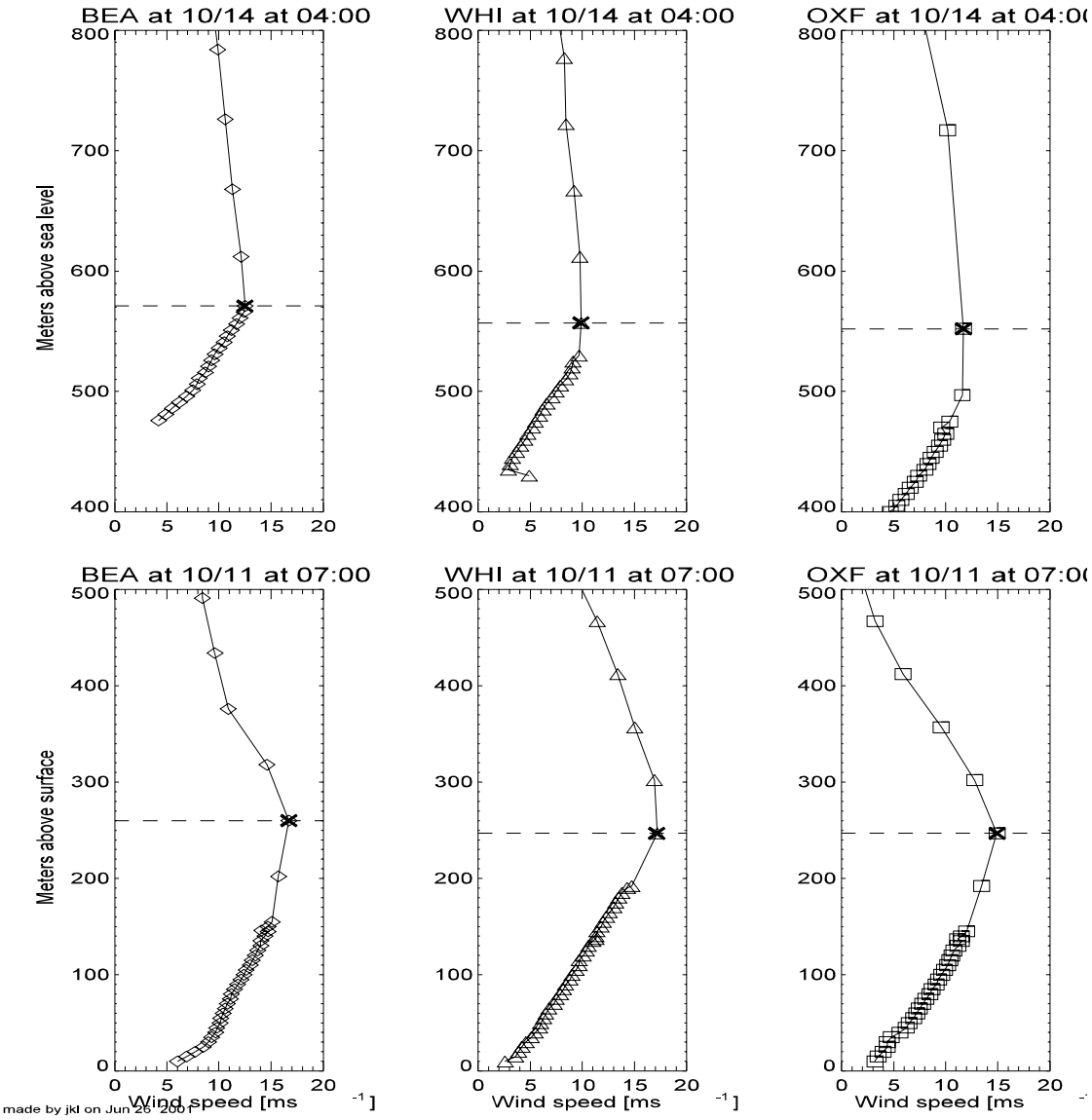

Figure 10: Regional variability of the low-level jet as seen in profiler/sodar data. The top three panels show wind speed profiles from 0400 UTC 14 October at Beaumont, Whitewater, and Oxford. The altitude has been adjusted for station elevation. The dotted line marks the level of the low-level jet as determined with the Andreas criterion with a wind speed difference of 1.5 m s^{-1}. All three sites show the jet at approximately 570 m MSL, indicating the jet height on this night is independent of terrain and approximately level. The bottom three panels depict wind speed profiles from 0700 UTC 11 October 2001; the altitude has not been adjusted for station elevation. The low-level jet at this time follows terrain quite closely, and is located at 250 m above the surface at all three sites.

4. Nighttime LLJ Evolution

Temporal behavior of LLJ characteristics have been hypothesized to be related to the appearance of turbulence and vertical mixing processes on the SBL near the surface, e.g., acceleration of the LLJ leads to increased shear and turbulence near the surface. To investigate these relationships it is thus critical to know how the LLJ evolves through the night. In this section we present time series of U_X, Z_X, and D_X through the night. The time series represent the *nighttime* behavior; the evening and morning transitions will be addressed in future studies. The analyses presented here were averaged over 15-min periods for HRDL and 1-h periods for sodar/profiler data. They begin at 0000 UTC, by which time the LLJ has at least begun to form, and on some evenings was fully formed, and they end at 1200 UTC.

4.1 TIME SERIES OF U_X, Z_X, and D_X

For presentation the nights have been divided into 4 categories: high wind (15-20 m s^{-1}), high-moderate winds (10-15 m s^{-1}), low-moderate wind (5-10 m s^{-1}), and low-wind (0-5 m s^{-1}) plus miscellaneous cases. Although these divisions seem arbitrary, similarities within and differences between groups suggest that they may be more functional. A Richardson number or similar characterization would be more appropriate, and a goal of future, more detailed case studies will be to determine more appropriate parameters to characterize LLJ behavior. The 4 categories and the nights that fell into each category are given in Table 2.

Table 2. Four categories of nights

UTC Night	Local Night October	Julian Night	IOP	Mean LLJ Speed (m/s) (VAD)
High wind nights				
25 Oct	24 - 25	298	-	15.2
27 Oct	26 - 27	300	12	14.6
28 Oct	27 - 28	301	-	13.2
High-moderate wind nights				
14 Oct	13 - 14	287	6	10.8
21 Oct	20 - 21	294	9	10.6
23 Oct	22 - 23	296	10	12.5
Low-moderate wind nights				
6 Oct	5 - 6	279	2	9.3
10 Oct	9 - 10	283	3	8.2
18 Oct	17- 18	291	7	6.8
24 Oct	23- 24	297	-	7.6
Light wind, misc. nights				
26 Oct	25 - 26	299	-	3.8
20 Oct	19 - 20	293	8	7.6
5 Oct	4 - 5	278	1	8.2

4.1.1 High-wind-speed jets (15-20 m s^{-1})

The nights when U_X was more than 15 m s^{-1} for at least 4 h (Fig. 11) also exhibited high turbulence levels for nearly all of the nighttime period after 0300 UTC, as indicated by values of $\overline{u'^2(z)}$ exceeding 0.4 m^2 s^{-2} below Z_X down to the surface, as determined by plots similar to Fig. 3 (not shown). On 25 and 27 Oct, U_X increased steadily through the night from 10 m s^{-1} at 02-03 UTC to 20 m s^{-1} by 11 UTC. 28 Oct had only a few hours of HRDL data, but profiler data indicated 20 m s^{-1} U_X values until 0800 UTC. The jet height Z_X was variable in time at the HRDL site and also variable between sites as indicated by the profiler data. Z_X tended to be above 100 m except at BEA (which was consistently lower than the other sites on 25 and 27 Oct), as the high wind speeds seemed mostly incompatible with very low jet heights. The direction tended to be steady, exhibiting a small amount of veering through the night.

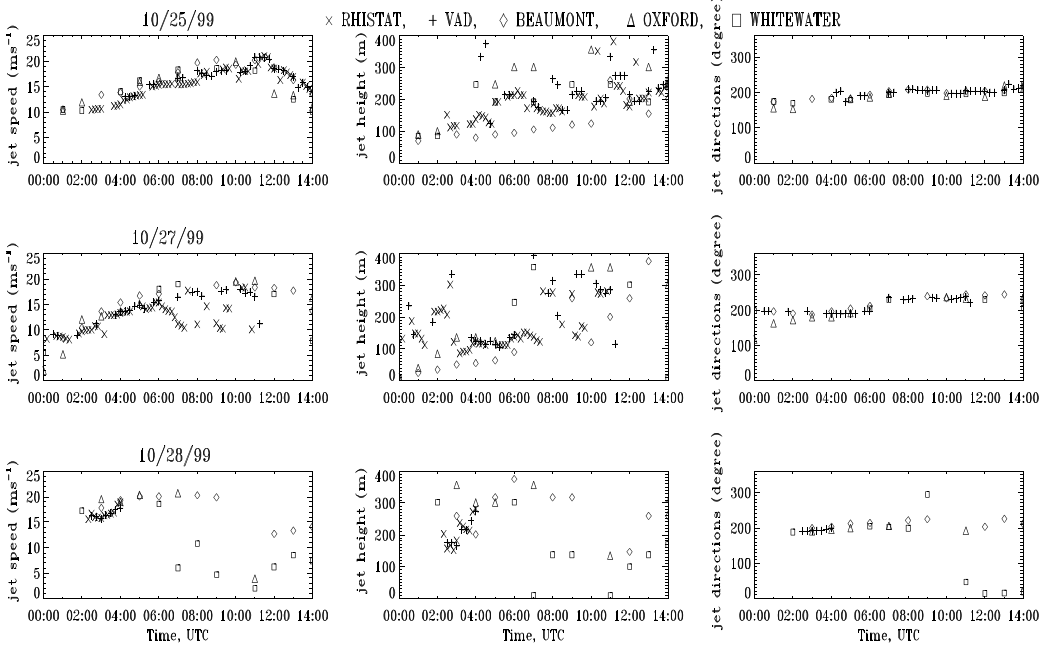

Figure 11: Time-series plots of LLJ characteristics for high-jet-speed (>15 m s^{-1}) nights: top row, 25 Oct; middle row, 27 Oct; and bottom row, 28 Oct. Abscissa is time of night in hour UTC. Ordinate of first (left) column is maximum jet speed U_X (m s^{-1}), second (middle) column is height of maximum speed Z_X, and third (right) column is wind direction at the level of maximum speed D_X. Symbols are as follows: × determined from HRDL vertical-slice scans, + determined from HRDL VAD-type scans, and open symbols represent sodar/profiler data from ◊ Beaumont (BEA), □ Whitewater (WHI), and ▵ Oxford (OXF).

4.1.2 High-moderate winds (10-15 m s^{-1})

On nights with high-moderate winds of >10 m s^{-1} for at least several hours (Fig. 12), U_X increased early in the evening until 0400 UTC. This occurred gradually on 14 and 23 Oct, but very suddenly (< ½ h) on 21 Oct. Z_X was generally above 100 m and again variable in time, and on 14 and 21 Oct, BEA tended to have the lowest Z_X. After 0700 UTC on 21 Oct discrepancies in the HRDL-measured jet heights were partly due to the development of a double jet structure, with one jet at ~150 m and another just below 300 m (see Fig. 1g). We can speculate that this is an example of LLJs at two different levels, responding to two different scales of horizontal pressure gradient–the lower jet to a more local scale, and the upper one to the Great-Plains-scale forcing. High $\overline{u_r'^2(z)}$ turbulence bursts below jet level occurred at times, but not as continuously as in the previous case. D_X veered strongly through the night on 14 Oct from NE to SE, and the other nights showed slight veering.

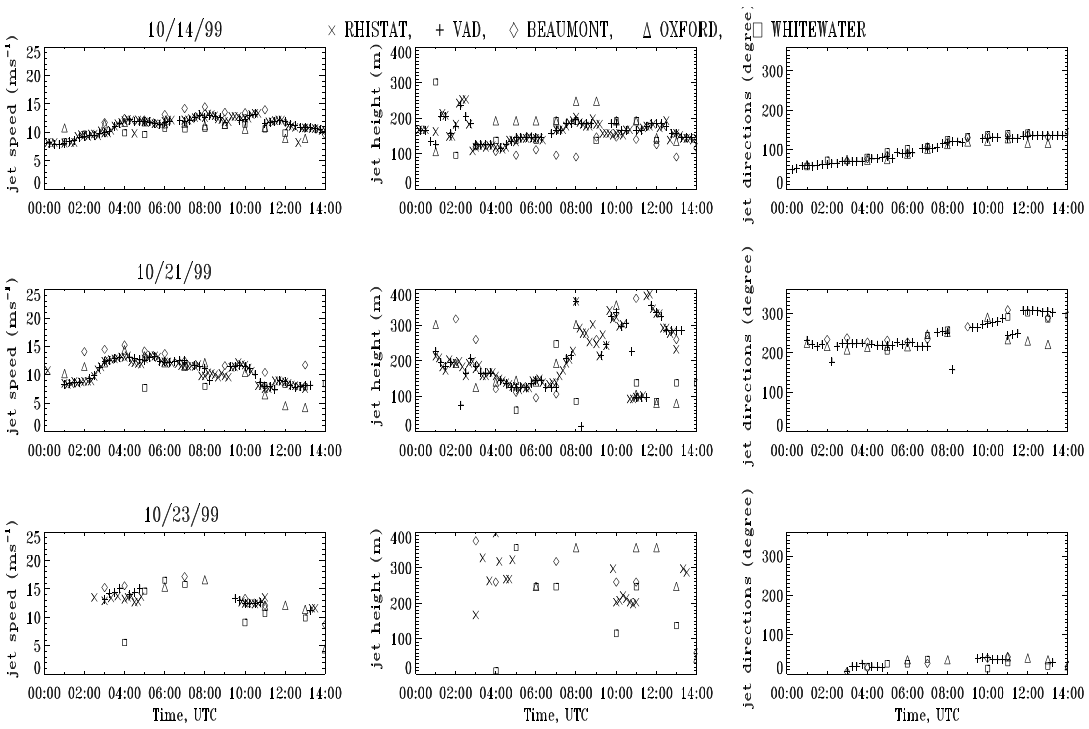

Figure 12: Time series plots of LLJ characteristics for high-moderate jet speed nights, as in Fig. 11. Top row, 14 Oct; middle row, 21 Oct; and bottom row, 23 Oct.

4.1.3 Low-moderate winds (5-10 m s^{-1})

On two of the four low-moderate wind nights (Fig. 13) U_X increased early in the evening, but on the other two nights (18 and 24 Oct) the peak speeds were remarkably steady all night from the start at 0000 UTC. Z_X was again much more variable both in time (as measured by HRDL) and in space than U_X. It tended to be at or just below 100 m, with upward excursions confined to under 200 m after 0200 UTC, i.e., no really high jets. Three of the 4 nights showed significant veering through the night. Although 24 Oct showed bursts of $\overline{u_r'^2}(z)$ exceeding 0.3 m^2 s^{-2} between the surface and Z_X after midnight (0600 UTC), on the whole these nights showed relatively low turbulence levels. An exception was a period of less than ½ h on 6 Oct around 0530 UTC, when shear-instability waves generated significant mixing just below Z_X, as reported by Newsom and Banta (2002) and Blumen et al. (2001). Another interesting night was 18 Oct, when 3 density-current or solitary-wave events were evident in the temperature and other records (Sun et al. 2002).

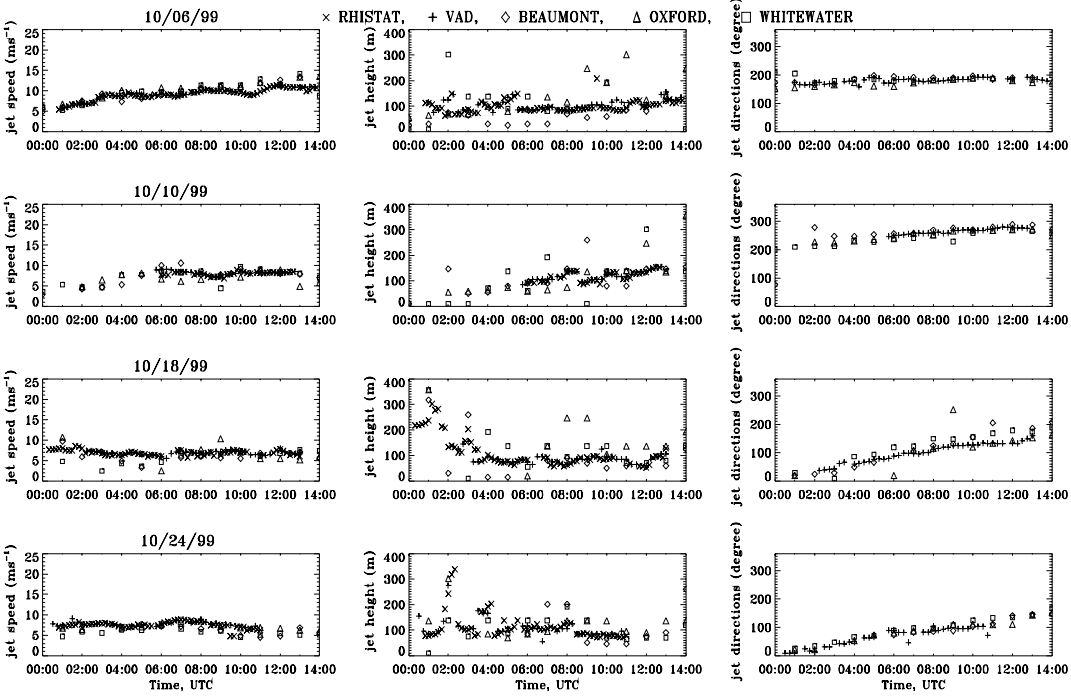

Figure 13: Time series plots of LLJ characteristics for low-moderate jet speed nights, as in Fig. 11. Top row, 6 Oct; second row, 10 Oct; third row, 18 Oct, and fourth (bottom) row, 24 Oct.

4.1.4 Low wind speeds (< 5 m s^{-1}) and miscellaneous cases

The only low-wind speed case (Fig. 14) was 26 Oct. In this case the LLJ selection criterion was important, because with a 2 m s^{-1} threshold requirement, many low-level wind maxima that we would want to include would be rejected, even though the profiles (e.g., Fig. 1c) often show a clear, low-level, evening maximum despite the slow speeds; thus, the 0.5 m s^{-1} criterion was more appropriate. This light-wind, low-level maximum showed up at all sites. Z_X was often difficult to determine and varied in time and space. After 0730 UTC the easterly drainage flow produced an increase in U_X at the HRDL site.

20 Oct was an unusual night that started out with a low, weak jet, but by midnight (local standard time: 0600 UTC) the speeds began to increase dramatically from a southerly direction. On 5 Oct, the first IOP night, U_X and Z_X appeared more variable than on other nights, and thus made it difficult to classify.

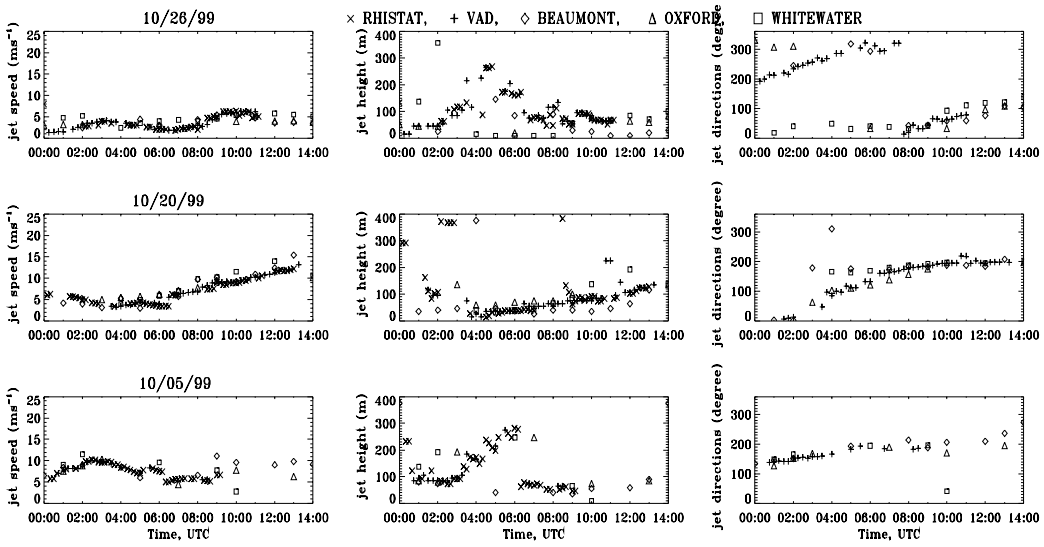

Figure 14: Time series plots of LLJ characteristics for low wind speed night and miscellaneous nights , as in Fig. 11. Top row, 26 Oct; middle row, 20 Oct; and bottom row, 5 Oct.

4.2 SMALLER-SCALE BEHAVIOR

The time series findings in the previous section were based on averaged quantities at 15-min intervals derived from HRDL data. Analyses based on individual scan data also showed interesting behavior at finer spatial resolution. For example, Fig. 15a shows quasi-periodic fluctuations in the speed and height of the LLJ as the jet speed ramps up early in the evening of 14 Oct. The period of these fluctuations was somewhat less than 10 min, and they may be associated with pressure fluctuations sensed at the surface (Cuxart, 2001, personal communication). Fig. 15b shows that these kinds of fluctuations were also present on 21 Oct, indicating that they may be part of the evening transition process. Fig. 15b also shows that the rapid increase in U_X noted in Fig. 12 actually took place between ~0225 and 0245 UTC, i.e., over a span of 20 min. The scan to-scan consistency in the trends of these quantities and the consistency between the vertical-slice scan data (RHISTAT) and the VAD-determined data give confidence that these fluctuations are real atmospheric phenomena.

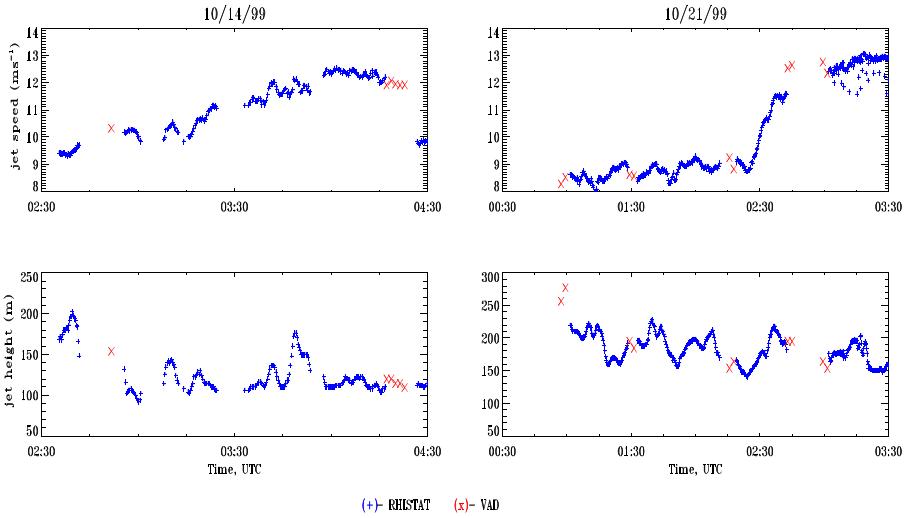

Figure 15: Time series of U_X (top) and Z_X (bottom) determined from individual HRDL vertical-slice (+) and VAD (×) scans, as opposed to averaged over a time interval as in the previous 4 plots. (a) 0230-0430 UTC on 14 Oct, and (b) 0030-0330 UTC on 21 Oct.

5. LLJ Turbulence Interactions

To illustrate the relationship between LLJ's and turbulence below the jet, we show data from two nights, a high-wind night (25 October) and a high-moderate wind night (21 Oct). Mahrt and

Vickers (2002) suggested two criteria for detecting when turbulence is predominantly being generated at levels above the surface and transported downwards, the "upside-down boundary layer": 1) TKE increasing with height and 2) the vertical turbulent flux of TKE being directed downward (i.e., negative).

These quantities were calculated from the 60-m tower data after high-pass filtering the data at 20 s, and are presented as time-height cross sections (Fig. 16).

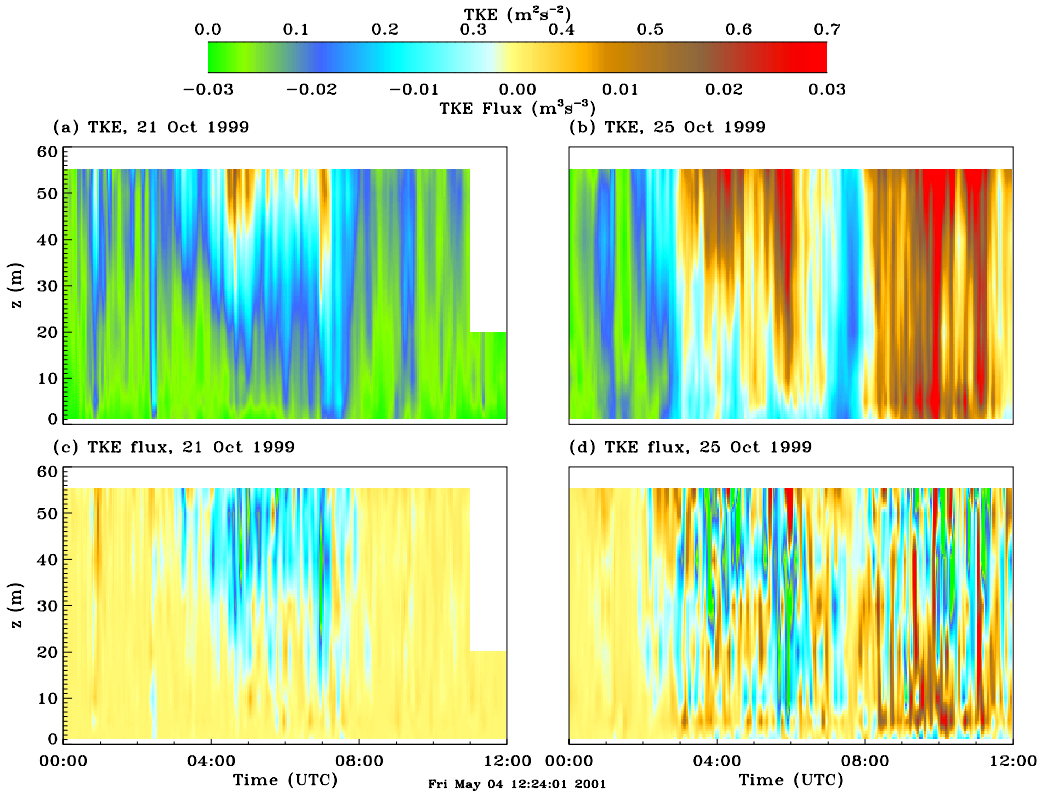

Figure 16. (a) TKE and (c) the vertical flux of TKE for the night of 21 Oct. 1999. (b) TKE and (d) the vertical flux of TKE for the night of 25 Oct. 1999. In (c) and (d) negative values imply downward mixing of TKE.

To compute TKE, each velocity component was detrended by high-pass filtering in the frequency domain. A six hour period of 20Hz data was FFTed. The resulting spectrum was set to zero for $|f|<f_{co}$. In this case the cut-on frequency f_{co} was chosen to eliminate fluctuations with periods longer than 20 s, so f_{co} = 1/20 Hz. This modified spectrum was then inverse transformed back into the time domain and the TKE was computed using a 40 s averaging period, oversampled at 20 s intervals.

The cross sections for 21 Oct, a night when the LLJ was mostly 10-13 m s^{-1}, show a period of high turbulence in the middle of the night between 04 and 08 UTC. TKE clearly increased with z during this episode, and the vertical TKE flux, which had very low values for most of the night, was strongly negative during the episode. Vertical profiles of these quantities at 0440 and 0700

UTC (Fig. 17a,b) show TKE increasing with z and negative TKE flux reaching a peak negative value near 30-40 m AGL, as found by Mahrt and Vickers (2002).

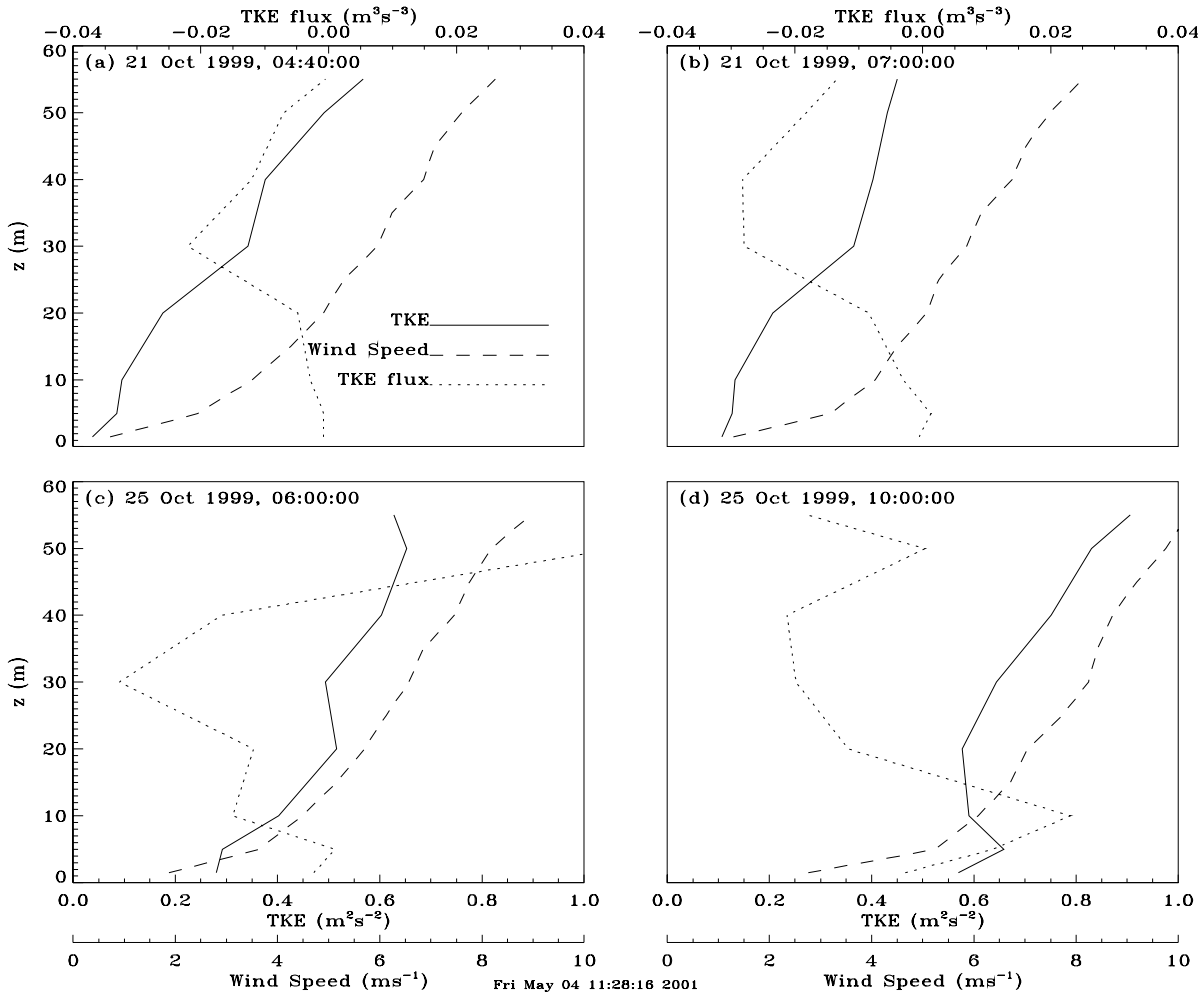

Figure 17. Representative profiles of TKE, TKE flux and mean wind speed for the night of 21 Oct 1999 (a and b) and the night of 25 Oct 1999 (c and d). Mean wind speeds were computed at twelve levels on 60-m tower using 40 s averages of both sonic anemometer and prop-vane data. TKE and TKE flux were computed from only the sonic anemometer data (eight levels).

On 25 Oct, the high-wind night, high levels of TKE were evident most of the time after 03 UTC. The pattern of relatively quiet turbulence levels before 03 UTC, followed by greater turbulence activity, was typical of many nights of CASES-99. The TKE pattern was complex, with periods of TKE increasing with height evident, especially above 30 m AGL, and other periods where TKE appeared to decrease with z, especially after 08 UTC and below 30 m. The TKE vertical-flux pattern was even more complex, with intermittent periods of both positive and

negative values. Sample profiles at 0600 (Fig. 17c) illustrate the increasing TKE with z and the negative TKE flux, as seen in the profiles in the 21 Oct case. Later profiles at 1000 UTC show decreases in TKE with z between ~5 and 20 m with positive TKE flux there, indicative of turbulence generated near the surface. Above 20 m, however, the behavior of TKE and TKE flux were as in the previous examples.

Overall, we find numerous examples of turbulence transported downward from jet level on nights with strong or moderately strong jets, in fact this behavior seems predominant during periods of strong turbulence. We also found evidence for the more normal behavior, when TKE decreased with height above the surface and TKE flux was positive. These occurrences, which indicate TKE being generated in the strong shear next to the surface and then exported upward, tended to be at lower levels, often below ~30 m, in agreement with the results of Mahrt and Vickers (2002). Obviously, we will learn much about the interaction between LLJ behavior and turbulent mixing below the jet by studying these and other cases individually in much greater detail.

7. Conclusions

This investigation of LLJ behavior and effects has taken advantage of two unique aspects of the CASES-99 dataset in south-central Kansas: the vertical and temporal resolution of the HRDL scan data and the location and separation of three sodar/profiler sites. The fine resolution of the HRDL data has allowed us to focus on the first wind speed maximum above the surface produced by nocturnal decoupling of the flow. This maximum is most likely responsible for the production of shear and the generation of turbulence between the surface and the LLJ, and understanding its behavior is believed critical to further understanding nighttime mixing processes between the atmosphere and the surface. The combination has allowed us to determine the overall typical characteristics (height Z_X, speed U_X, and direction D_X) of the LLJ's seen during the October 1999 experiment, to investigate the spatial variability of the LLJ characteristics over the 60-km watershed study area, to study the evolution of LLJ characteristics through many nights, and to look at the relationship between the LLJ and turbulence properties on two study nights.

The overall behavior was characterized by determining the frequency of occurrence of the various characteristics. The mode in the U_X histogram at the main site was at 8-9 m s^{-1}, but this was site dependent: the highest site tended to have the fastest speeds and the lowest site, the slowest speeds. The high frequency of jets with Z_X near and below 100 m AGL is potentially significant for wind-energy applications. Comparisons between data for the 3 sites at individual hours showed that the U_X and D_X tended to be similar across the region, but Z_X was more variable in space. Z_X at the highest station (BEA) tended to be lowest, indicating that in general the jet was not terrain following, but it could be close to level at least at times. These findings indicate that the structure of the LLJ was as a sheet or extensive layer of high-momentum flow over the entire region.

The time series of jet characteristics showed that, except for the strongest wind cases, U_X tended to be relatively constant, whereas Z_X was much more variable. This suggests that changes in the shear below the jet could be due to changes in the height rather than the speed of the jet.

High time resolution achieved by plotting data from individual HRDL scans showed that the speed and height sometimes fluctuated on time periods of several minutes. Whether these undulations have an effect on processes near the surface is under investigation. During several periods of high turbulence noted in the analysis of Doppler lidar data, we found that these events were characterized by turbulence generated aloft and transported downward, in accordance with the so-called upside-down boundary layer model.

An overall objective of CASES-99 was to understand, and then suggest ways to model and parameterize, turbulence in the SBL. Characterization of the LLJ in space and time is seen as one of several first steps. Important next steps are using individual case studies and case-study events (such as Blumen et al. 2001, Newsom and Banta 2002, Sun et al. 2002, Mahrt and Vickers 2002) to further probe the role of turbulence generated in the shear below the jet in the vertical transport of quantities between the surface and the atmosphere. Another important next step is to determine what controls the behavior of the LLJ on a given night.

Acknowledgments. Funding for analysis and field measurements was provided by the Army Research Office under proposal #40065-EV, and the Center for Geosciences/Atmospheric Research at Colorado State University. The National Science Foundation (Grants # ATM-9908453 [HRDL] and # ATM-9903645 [JKL]) also provided funding for the field measurements and analysis of sodar/profiler measurements. The authors are indebted to: J. Otten, Dr. W. Eberhard, and M. Pichugin for assistance with HRDL data acquisition; Dr. V. Wulfmeyer, S. Sandberg, J. George, Dr. W. A. Brewer, A. Weickmann, R. Richter, and Dr. R. M. Hardesty for HRDL preparation and setup; Dr. J. Sun, S. Burns, Dr. S. Oncley, and N. Chamberlain for tower and sounding data; Dr. G. Poulos, Dr. W. Blumen, and Dr. D. Fritts for organizing the CASES-99 field project, J. Klazura for local arrangements, and J, Lucas and other ANL personnel for the profiler/sodar data.

References

Andreas, E.L., Claffey, K.J., and Makshtas, A.P., 2000: Low-Level Atmospheric Jets and Inversions over the Western Weddell Sea. Boundary-Layer Meteor., **97**, 459-486.

Blackadar, A.K., 1957: Bounday Layer Wind Maxima and Their Significance for the Growth of Nocturnal Inversions. Bull. Amer. Meteor. Soc., **38**, 283-290.

Blumen, W., Banta, R.M., Burns, S.P., Fritts, D.C., Newsom, R.K., Poulos, G.S., and Sun, J., 2001: Turbulence Statistics of a Kelvin-Helmholtz Billow Event Observed in the Nighttime Boundary Layer during the CASES-99 Field Program. Dyn. Atmos. Oceans, in press.

Bonner, W.D., 1968: Climatology of the Low Level Jet. Mon. Wea. Rev., **96**, 833-850.

Bowen, B.M., 1996: Example of Reduced Turbulence during Thunderstorm Outflows. J. Appl. Meteor., **35**, 1028-1032.

Coulter, R. L,. and Kallistratova, M.A., 1999: The Role of Acoustic Sounding in a High-Technology Era. Meteorol. Atmos. Phys., **71**, 3-13.

Coulter, R. L., Klazura, G., Lesht, B.M., Martin,T.J., Shannon, J.D., Sisterson, D.L,. and Wesely, M.L., 1999: The Argonne Boundary Layer Experiments Facility: Using minisodars to complement a wind profiler network. Meteorol. Atmos. Phys., **71**, 53-59.

Eklund, W.L., Carter, D.A., and Balsley, B.B., 1988: A UHF Wind Profiler for the Boundary Layer: Brief Description and Initial Results. J. Atmos. Oceanic Technol., **5**, 432-441.

Grund, C.J., R,M. Banta, J.L. George, J.N. Howell, M.J. Post, R.A. Richter, and A.M. Weickmann, 2001: High-Resolution Doppler Lidar for Boundary-Layer and Cloud Research. J. Atmos. Ocean. Technol., **18**, 376-393.

LeMone, M.A., et al., 2000: Land-Atmosphere Interaction Research, Early Results, and Opportunities in the Walnut River Watershed in Southeast Kansas: CASES and ABLE. Bull. Amer. Meteor. Soc., **81**, 757-779.

Lundquist, J.K., 2000: The Evening Transition of the Atmospheric Boundary Layer: Inertial Oscillations, and Boundary-Layer Dynamics. Ph.D. Dissertation, University of Colorado at Boulder, 180 pp.

Mahrt, L., 1999: Stratified Atmospheric Boundary Layers. Boundary-Layer Meteor., **90**, 375-396.

Mahrt, L., and Vickers, D., 2002: Contrasting Vertical Structures of Nocturnal Boundary Layers. Boundary-Layer Meteor , submitted.

Mitchell, M.J., Arritt, R.W., and Labas, K., 1995: A Climatology of the Warm Season Great Plains Low-Level Jet Using Wind Profiler Observations. Wea. Forecasting, **10**, 576-591.

Newsom, R.K., and Banta, R.M., 2002: Shear Instability Gravity Waves in the Stable Nocturnal Boundary Layer as Observed by Doppler Lidar during CASES-99. J Atmos. Sci., submitted.

Poulos, G.S., et al., 2002: CASES-99: A Comprehensive Investigation of the Stable Nocturnal Boundary Layer. Bull. Amer. Meteor. Soc., submitted.

Smedman, A.S., 1988: Observations of a Multi-Level Turbulence Structure in a Very Stable Atmospheric Boundary Layer. Boundary-Layer Meteor , **44**, 231-253.

Sun, J., et al., 2002: Intermittent Turbulence in Stable Boundary Layers and its Relationship to Density Currents and Solitary Waves. Boundary-Layer Meteor , submitted.

Whiteman, C. D., Bian, X., and Zhong, S., 1997: Low-Level Jet Climatology From Enhanced Rawinsonde Observations at a Site in the Southern Great Plains. J. Appl. Meteor., **36**, 1363-1376.

Wulfmeyer, V.O., Randall, M., Brewer, W.A., Hardesty R.M., 2000: 2 μm Doppler Lidar Transmitter with High Frequency Stability and Low Chirp. Opt. Lett., **25**, 1228-1230.

Zhong, S., Fast, J.D., and Bian, X., 1996: A Case Study of the Great Plains Low-Level Jet Using Wind Profiler Network Data and a High-Resolution Mesoscale Model. Mon. Wea. Rev., **124**, 785-806.